引用格式：WANG Muguang, GAO Pufeng, CAI Shiyi, et al. Recent Progress in Microwave Photonic Magnetic Field Sensing Technology (Invited)[J]. Acta Photonica Sinica, 2026, 55(3):0355105
王目光,高浦峰,蔡诗怡,等.微波光子磁场传感技术研究进展(特邀)[J].光子学报,2026,55(3):0355105

微波光子磁场传感技术研究进展(特邀)

王目光,高浦峰,蔡诗怡,樊庆赓,张乃晗
(北京交通大学 光波技术研究所 全光网络与现代通信网教育部重点实验室,北京 100044)

摘　要:为突破传统电学磁场传感器在复杂电磁环境中的性能瓶颈,本文系统综述了微波光子磁场传感技术的研究进展与发展趋势。微波光子磁场传感技术通过将磁场导致的光信号变化通过微波光子链路进一步映射至微波域,从而实现高性能磁场测量。本文重点阐述了微波光子磁场传感技术的核心原理及演变路径,包括光电振荡器与微波光子滤波器传感系统,分析其在提升磁场灵敏度、响应度、分辨率及动态响应方面的关键作用。同时,结合神经网络建模与误差补偿算法,讨论了非线性迟滞、温度串扰与系统噪声对测量性能的影响及其抑制策略。微波光子磁场传感技术能够实现静态、交流及矢量磁场的高分辨快响应测量,结合信号处理技术可以显著增强系统的抗干扰能力与环境适应性,为电力监测、空间探测及生物医学等领域提供高性能解决方案,并推动磁场传感技术向微型化与智能化方向发展。

关键词:光纤传感器;磁光系统;振荡器;光谱学,微波
中图分类号:TP212.1　　**文献标识码**:A　　**doi**:10.3788/gzxb20265503.0355105

0　引言

磁场作为自然界的基本物理场之一,在导航、医疗、空间探测等领域具有重要作用[1-4]。随着物联网、生物医学成像和智能电网等技术的快速发展,磁场传感器不仅需要具备更高的灵敏度和分辨率[5],还应满足复杂环境、极端温度及分布式监测等应用需求。

磁场传感技术已形成多种技术路线。电磁感应式传感器具有宽动态范围,但体积庞大且低频响应有限;霍尔效应传感器依赖半导体工艺,易受温度漂移影响[6];磁阻效应传感器虽具高灵敏度,但制备复杂、成本较高[7-8];超导量子干涉仪可实现飞特斯拉级灵敏度[9],却受限于低温冷却系统,难以大范围推广应用。随着磁场测量场景日益复杂,如电力设备局部磁场监测、生物脑磁成像及深海地磁探测等[10-12],传统传感器的性能瓶颈愈发突出,亟需新型高灵敏度、宽带、抗干扰的磁场传感方案。

光纤磁场传感技术为磁场探测提供了新的思路。光纤以光波为载体,具有体积小、成本低、耐腐蚀等优势[13]。光纤磁场传感原理主要利用磁光晶体、磁流体或磁致伸缩材料等磁场换能单元,将磁场信息调制至光信号中,典型代表包括基于法拉第旋光效应的光纤磁场传感器[14-15],基于磁致伸缩材料与光纤布拉格光栅(Fiber Bragg Grating, FBG)协同结构的磁场测量系统,以及基于磁性纳米流体与光纤干涉仪构建的高灵敏度磁场传感器等[16-19]。此类光纤传感器不仅具备良好的可重构性,还可通过复用实现矢量磁场测量,已在智能电网、海洋监测及生物磁测中展现出应用潜力。

然而,光纤磁场传感技术在灵敏度、带宽与响应速度等方面仍存在局限。为突破瓶颈,微波光子技术将光纤传感固有优势与微波信号的高精度快响应测量相结合,为磁场高精度探测提供了新途径[20-21]。其中,基于光电振荡器(Optoelectronic Oscillator, OEO)的磁场传感系统通过将磁场变化映射为微波频率漂移,实现高灵敏度与低噪声解调;基于微波光子滤波器(Microwave Photonic Filter, MPF)的方案则利用磁场调谐滤波响应以实现微波域测量[22-24]。该类技术具备宽频响应、高分辨率和快速响应等优点,能够适应从地磁到高

基金项目:国家自然科学基金(62371035, U2006217)
第一作者(通讯作者):王目光,mgwang@bjtu.edu.cn
收稿日期:2025-12-23;**录用日期**:2026-01-05

频电磁测量的多场景应用。

当前磁场传感仍面临若干挑战，包括亚nT级弱磁信号的高灵敏检测、长距离传输下的解调稳定性以及复杂环境下的抗干扰能力等[25-26]。未来，随着新型磁光材料、片上集成光子器件及智能信号处理算法的融合发展，磁场传感技术也在向高灵敏度、强环境适应性与智能化方向发展[27-28]。例如，二维磁光材料的出现将显著增强光磁耦合，而人工智能辅助的实时解调算法可提升复杂场景下的系统稳定性。需要说明，不同文献中对磁场传感性能参数的定义及测试条件可能存在差异。本文中，“响应度”统一指外加磁场变化引起的待测电信号或光信号的变化率，通常以Hz/mT或pm/mT表示。“灵敏度”指在测量带宽内系统可测量的最小磁场变化，通常以nT/Hz$^{1/2}$或pT/Hz$^{1/2}$表示。本文中所列性能参数均直接引自原文报道结果，其具体定义和测试条件以对应文献为准。

本文围绕微波光子磁场传感的关键技术展开综述。概述基于OEO与MPF的磁场传感技术及其基本原理，重点分析相关架构在灵敏度、分辨率、动态响应及多参量解耦方面的性能优化方案。讨论磁滞补偿与噪声抑制等信号后处理方法在提升测量精度与系统稳定性中的作用。最后，对微波光子磁场传感技术面临的关键挑战及未来发展方向进行分析与展望。

1 微波光子磁场传感技术

电学磁场传感器如磁通门[29]、磁阻[30]、霍尔效应[31]及超导量子干涉器件[32]等，虽已实现应用，但仍存在结构复杂、抗干扰能力差及环境适应性有限等问题，难以满足复杂场景下的高精度磁场测量需求。为此，融合光学与微波优势的微波光子磁场传感技术应运而生。该类传感系统通过将磁场导致的光信号变化映射至微波域，实现高精度、宽带和低噪声的磁场测量。相较于纯光学解调方式，微波光子磁场传感在分辨率、动态带宽及响应速度方面具有显著优势[33-35]。其基本原理是：磁场变化调制光信号的波长、相位或强度，利用微波光子链路进一步映射为微波信号的频率或相位等参量变化，并在微波域实现精确解调。目前，微波光子磁场传感系统主要包括基于OEO和基于MPF的磁场传感两种典型技术路线。前者依赖高Q振荡环路把光路或光信号变化转换为频率或相位漂移，后者则把磁场引起的光信号变化映射为滤波器中心频率或幅频响应的可测变化。二者在实现路径与性能上各有侧重且相互补充。

OEO自1994年提出以来因其高Q值与低相位噪声而广泛用于高性能微波生成与精密测量[36-38]。基于OEO的磁场传感系统通常由光源、电光调制器（Electro-Optic Modulator，EOM）、光纤磁场传感单元、单模光纤（Single Mode Fiber，SMF）、光电探测器（Photodetector，PD）、电带通滤波器（Electric Bandpass Filter，EBPF）以及电放大器（Electric Amplifier，EA）构成，如图1所示。磁场传感单元将外磁场信息映射至光信号波长或相位等参量信息上，光信号经光电探测后转化为电信号，并通过EBPF与EA构成闭环反馈。其中，SMF为OEO环路提供长时延以提升等效品质因数，从而降低振荡信号的相位噪声；EBPF用于选择振荡模式，确保系统工作在单模振荡状态；EA为环路提供足够增益以满足自激振荡条件。当磁场传感单元嵌入OEO环后，外界磁场将引起OEO振荡频率或相位的变化。通过电谱分析仪（Electrical spectrum analyzer，ESA）或数字信号处理（Digital Signal Processing，DSP）技术对该变化进行测量，即可实现磁场传感。根据

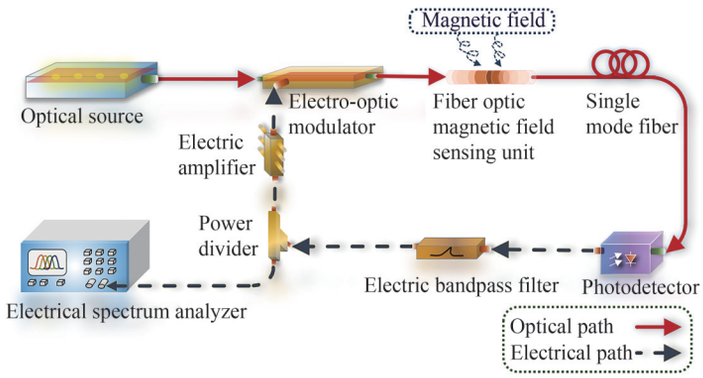

图1 基于OEO的磁场传感结构

Fig.1 Schematic diagram of magnetic field sensing structure based on OEO

不同待测磁场类型，可将OEO磁场测量技术分为直流磁场测量与交流磁场测量两类。前者主要关注静态或缓变磁场下的高分辨响应及磁-温解耦问题，后者则着重于交变磁场频谱下的解调方法与灵敏度优化。

1.1 基于OEO的直流磁场传感技术

在直流磁场测量中，OEO结构主要通过光学干涉、波长漂移或谐振频率变化来实现磁-光-微波映射。针对高响应度磁场测量以及温度交叉敏感解耦的需求，下面重点介绍三类代表性研究工作：磁场增敏结构、磁-温双参量测量结构以及改进型OEO磁场传感结构设计。

磁场增敏可通过结构优化、应力调控或复合腔增强实现。2024年，WU Beilei等利用丙烯酸酯粘合剂构建的非本征型法布里-珀罗（Fabry-Perot，FP）-FBG腔实现相位-强度转换[39]，并将其粘附在巨磁致伸缩材料（Giant Magnetostrictive Materials，GMM）表面以引入磁致伸缩效应，磁场响应度达到4.86 GHz/mT，相比本征型FP-FBG提升约6倍，其结构如图2(a)所示。刘仟等采用空气腔FP-FBG结构进一步降低界面反射损耗与封装残余应力，在20.2～21.8 mT范围内实现4.258 GHz/mT的磁场响应度[40]，如图2(b)所示。此外，GAO Pufeng等通过设计增敏封装结构增强了GMM的磁致伸缩系数，从而显著提高了磁场响应度[41]。该方案采用一种预应力-预磁化复合封装结构，在外加磁场作用前对GMM同时施加机械预应力与磁偏置场，从而显著增强其有效磁致伸缩系数。FBG固定于该封装结构的外表面，构成整体式磁场传感单元，如图2(c)所示。外加磁场会诱导GMM产生形变，从而引起FBG中心波长发生变化。该波长变化进一步通过环路内的色散介质映射为OEO振荡频率的可测漂移，实现对磁场的高响应解调。实验结果表明，采用该特异性增敏封装结构后，系统磁场响应度较未封装结构提升约16.3倍。上述结果进一步表明，FBG与GMM之间的机械耦合效率对磁场响应度与测量范围起着关键作用。

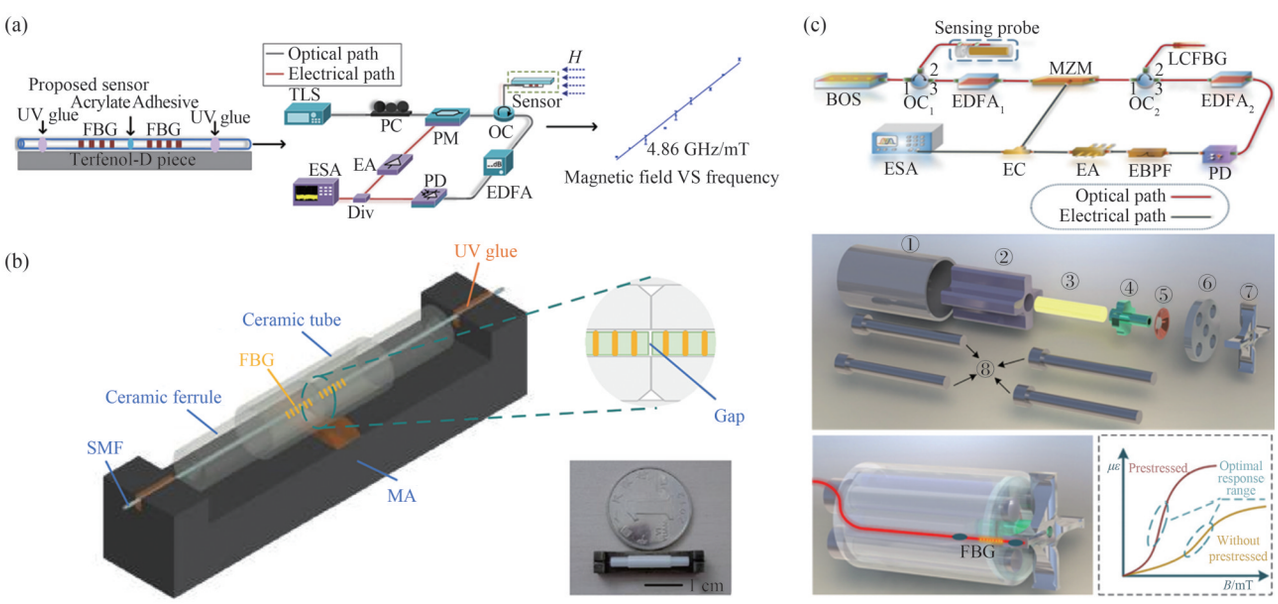

图2 响应度增强型传感单元设计。(a) 非本征型FP-FBG传感器结构及其实验响应度[39]；(b)空气腔FP-FBG传感器结构及其实验响应度[40]；(c)预应力预磁化增强响应度传感器结构及其实验响应度[41]

Fig.2 Responsivity enhanced sensor design. (a) Extrinsic FP-FBG sensor structure and its experimental responsivity[39]; (b) Air cavity FP-FBG sensor structure and its experimental responsivity[40]; (c) Prestressed and pre-magnetized enhanced-responsivity sensor structure and its experimental responsivity[41]

为提高基于OEO的磁场传感响应度，采用游标效应进行响应度放大是行之有效的方案之一。2022年，SUN Wei等提出了一种基于FBG和双环OEO的高精度磁场传感器[42]。通过将蚀刻后的FBG与磁流体（Magnetic Fluid，MF）结合，利用OEO将磁场变化转换为振荡频率的变化进行测量。该传感系统在5～10 mT的范围内，实现了响应度和最大测量误差分别为16.3 Hz/Oe和±0.05 mT的高性能磁场测量。WU Beilei等提出并通过实验证明了一种基于双环OEO的高响应度磁场测量方法[43]。该双环OEO使用级联GMM-FBG和蒙乃尔合金（Monel alloy）-400-FBG两个传感单元。OEO环路包含来自双FBG的两个反射信号，作为注入具有不同光纤长度的两个路径的独立光源。环路中引入的色散使GMM-FBG的波长偏移可以转换为OEO腔内

微波信号的频率偏移。与传统的单环配置不同，所提出的OEO由于两个环路之间的长度差异而产生游标效应。实验结果表明，磁场响应度提高了40倍。由于Monel-400合金的热膨胀系数与GMM相近，因此可减轻磁场测量中的温度串扰。与使用未处理的参考FBG相比，温度引起的磁场误差从2.46 mT降低到0.06 mT。

OEO也可用于多参量协同测量。2018年，WU Beilei等提出了双频OEO结构，利用相位-强度转换构建双通带MPF可同时获得两路振荡与拍频信号，并将磁场与温度分别映射到频移量上，如图3(a)所示[33]。以GMM-FP-FBG和FP-FBG分别作为磁场与温度传感单元，实验得到38.4 MHz/Oe的磁场响应度与1.21 GHz/℃的温度响应度，同时监测两振荡频率即可实现磁场温度双参量同时测量。为实现温度补偿，ZHANG Naihan等提出一种将马赫-曾德尔干涉仪(Mach-Zehnder interferometer, MZI)嵌入OEO的方案[44]，通过在MZI的一臂粘贴GMM并精确匹配另一臂长度以抑制温度漂移，如图3(b)所示。在21～41 ℃范围内，温度引起的频移仅120 kHz，相较未补偿降低3个数量级。在此基础上，CAI Shiyi等融合有限冲激响应与无限冲激响应MPF的混合结构，并引入极限学习机(Extreme Learning Machine, ELM)进行频谱识别[45]，如图3(c)所示。该方案在0～45 mT范围内实现磁场-温度同时解调，其响应度分别达到68.3 kHz/mT与5.37 MHz/℃。此外，FENG Danqi提出了波分复用(wavelength division multiplexing, WDM)双环OEO结构[46]。该方案在同一环境下构建互为基准的双通道，实现了磁场与温度的同时测量，并有效抑制了温度串扰。实验结果表明，其磁场和温度响应度分别达到250 Hz/Oe和1.97 kHz/℃，如图3(d)所示。

改进型OEO磁场传感结构也被关注，如图4所示。GU Sanfeng等提出了一种基于双环OEO与紧凑型同轴模式干涉仪(Mode Interferometer, MI)串联的高精度磁场传感器[47]。研究人员设计了一种高灵敏度光纤磁场探头，由涂覆MF的锥形双模光纤夹在两段单侧纤芯偏移的SMF之间构成，利用干涉仪的光谱切割效应实现了光源的波长调谐，其结构如图4(a)所示。实验中制备了芯偏移距离为5 μm，腰部直径为9.2 μm

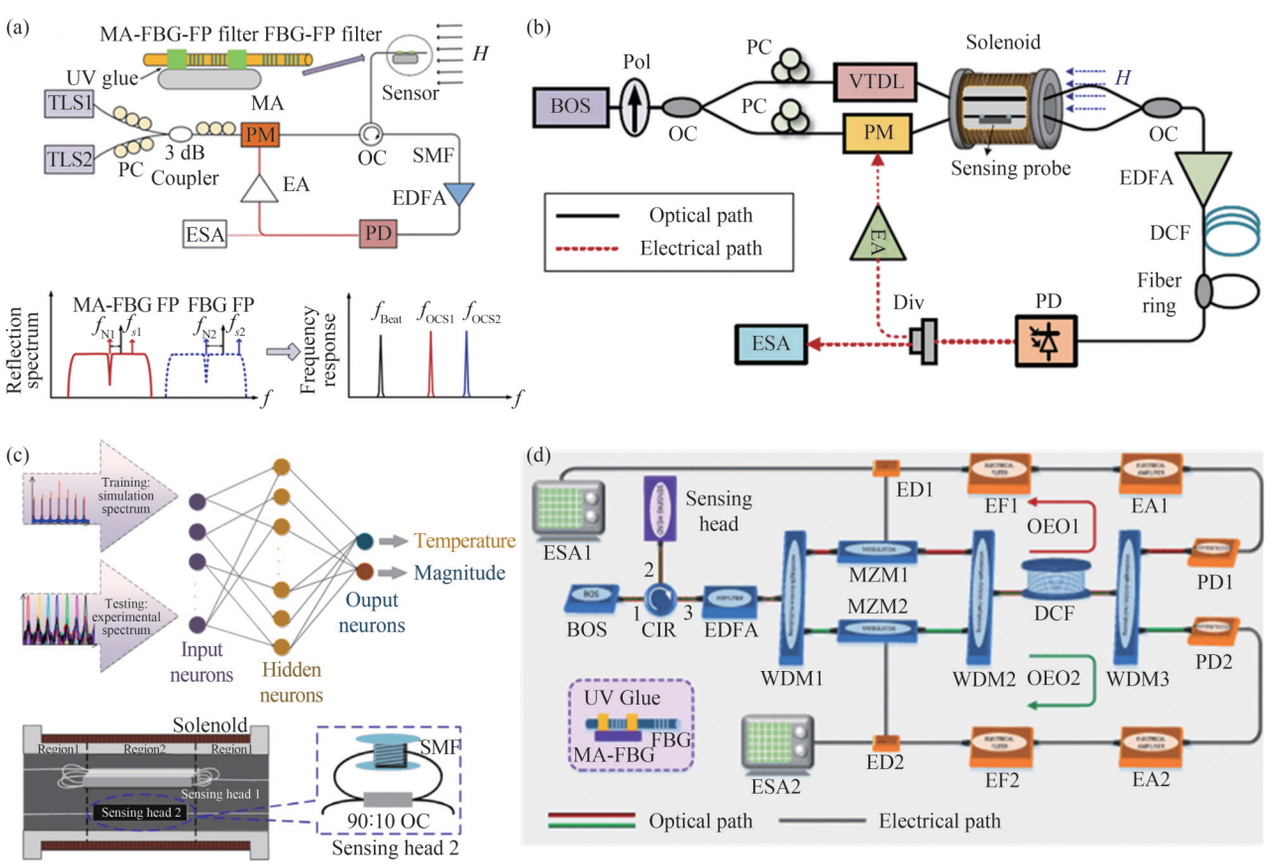

图3 基于OEO的磁温双参量传感结构。(a)双频光电振荡器实验结构及传感原理[33]；(b)MZI嵌入式光电振荡器磁场传感结构[44]；(c)基于ELM辅助光电振荡器的双参数传感器[45]；(d)基于WDM的OEO磁场-温度传感结构[46]

Fig.3 OEO-based magnetic-temperature dual-parameter sensing structure. (a) Dual-frequency OEO experimental structure and sensing principle[33]; (b) MZI embedded OEO magnetic field sensing structure[44]; (c) Dual parameter sensor based on ELM assisted OEO[45]; (d) WDM-based OEO magnetic field and temperature sensing structure[46]

的同轴MI。将设计的同轴MI嵌入双环OEO系统中，在6.69～8.35 mT范围内实验得到磁场响应度为－1.508 kHz/mT，对应测量误差在±0.089 mT以内。此外，除采用传统OEO磁场传感外，还可以采用耦合光电振荡器（Coupled Optoelectronic Oscillator，COEO）来实现。FENG Danqi等提出了一种基于COEO的磁场传感结构[48]，如图4(b)所示。COEO具有两个相互耦合的环：光纤激光器环和OEO环。在光纤激光器环中，偏振模拍频（Polarization Mode Beat，PMB）信号由其环路双折射决定。在OEO回路中，产生一个其频率等于PMB信号的微波信号。将磁光晶体插入到COEO环路中，引入了磁场相关的双折射变化。上述直流磁场测量方案表明，通过结构优化与多参量补偿，OEO可在维持高频稳定性的同时实现优异的响应度与抗温漂性能。

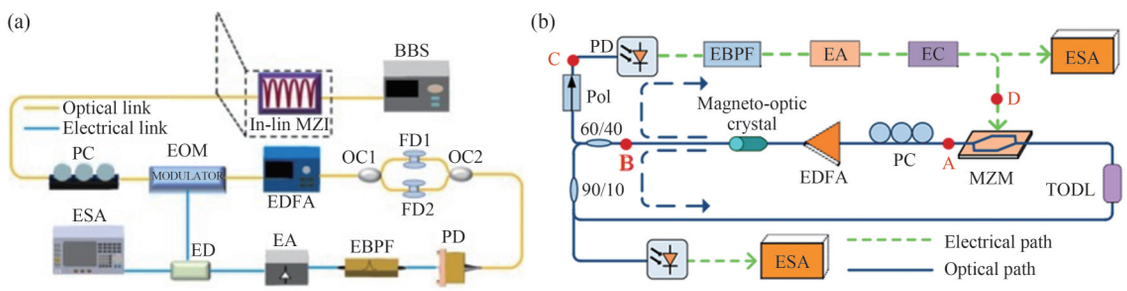

图4　基于改进OEO的直流磁场传感结构。(a)双环OEO和紧凑型MI的磁场传感器[47]；(b)嵌入磁光晶体的COEO磁场传感结构[48]

Fig.4　Novel DC magnetic field sensing structure based on OEO. (a) Magnetic field sensor cascaded between a dual loop OEO and a compact coaxial MI[47]; (b) COEO magnetic field sensing structure with embedded magneto-optical crystal[48]

1.2　基于OEO的交流磁场传感技术

当外磁场随时间变化时，OEO可将磁致伸缩引起的光学调制转化为振荡信号的相位或频率调制，实现交变磁场的动态测量。与直流测量相比，交变磁场测量更关注系统的测量带宽、相位噪声及低噪解调性能。2025年，GAO Pufeng等提出了一种基于OEO的交流磁场传感方案，其中将绑定于GMM表面的FBG反射光直接作为OEO的光源[49]。通过在GMM施加交流磁场，交流磁场信息被有效映射至OEO射频振荡信号的相位变化中，实现了100～9 600 Hz频率范围内的交变磁场解调，如图5(a)所示。实验结果表明，在磁场频率为1 350 Hz时，磁场响应度与灵敏度分别为327.3 rad/mT和4.65 nT/Hz$^{1/2}$，验证了OEO在交流磁场测量中的高灵敏解调能力。

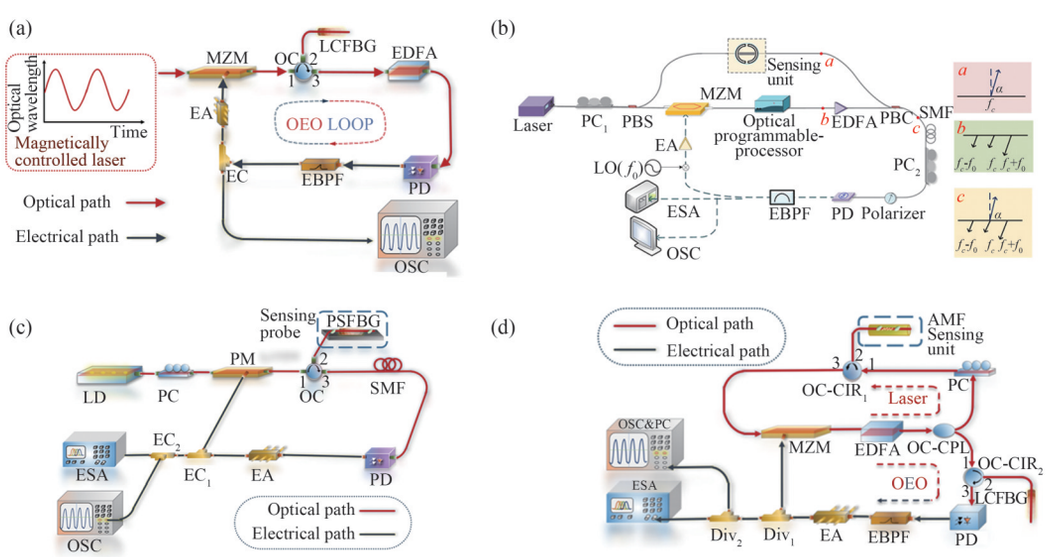

图5　基于OEO的交流磁场传感结构。(a)基于色散效应的OEO结构[49]；(b)内嵌MZI传感单元的OEO结构；(c)相位-强度转换的OEO结构；(d)COEO交流磁场传感系统

Fig.5　OEO-based AC magnetic field sensing structures. (a) OEO structure based on dispersion effect[49]; (b) OEO structure with embedded MZI sensing unit; (c) OEO structure with phase-intensity conversion; (d) COEO-based AC magnetic field sensing system

在此工作基础上，本课题组进一步提出了多种基于OEO的交流磁场传感方案。其一，通过将SMF缠绕于GMM表面并作为干涉臂嵌入OEO环路，实现了将交流磁场诱导的磁致形变映射为OEO振荡信号的相位变化。该结构在1～14 kHz的磁场频率范围内实现了1 nT/Hz$^{1/2}$@10 kHz的磁场灵敏度，如图5(b)所示。其二，基于相移光纤布拉格光栅(Phase-Shifted FBG，PS-FBG)下陷峰的波长漂移特性，可将交变磁场信息映射为OEO振荡信号的频率偏移，如图5(c)所示。实验结果表明，在500～10 kHz的测量频率范围内，相位时域波动约为±0.4 rad，磁场灵敏度达到0.509 pT/Hz$^{1/2}$@2 000 Hz，实现了pT量级高灵敏度磁场探测。此外，本课题组还提出了一种基于COEO的交流磁场传感方案，如图5(d)所示。该方案利用磁场传感单元GMM-FBG引发锁模环路的相位扰动，并将其转化为OEO振荡信号的相位波动。在240～10 100 Hz的频率范围内，实现了磁场响应度与灵敏度分别为3.64 rad/mT与24.78 nT/Hz$^{1/2}$的高性能磁场传感。

综上所述，以上交流磁场测量充分发挥了OEO在相位噪声与快响应等方面的固有优势。通过构建高性能OEO磁场传感系统，可实现pT/Hz$^{1/2}$量级的高灵敏度磁场测量。基于OEO的微波光子磁场传感技术在静态高精度磁场测量与动态弱磁场传感等应用场景中均展现出优异的综合性能。表1汇总了部分代表性

表1 基于OEO的微波光子磁场传感技术参数对比

Table 1 Comparison of microwave photon magnetic field sensing technology parameters based on OEO

Scheme	Sensing structure	Magnetic field responsivity	Magnetic field sensitivity	Temperature responsivity	Magnetic field range	Temperature compensation performance	References
Dual-frequency OEO	GMM-FP-FBG	38.4 MHz/Oe	/	1.21 GHz/℃	20～70 Oe	/	[33]
PM-IM OEO	GMM-FP-FBG with acrylate adhesive	4.86 GHz/mT	/	10.8 GHz/℃	1.7～2.58 mT	/	[39]
PM-IM OEO	Air-cavity GMM-FP-FBG	4.258 GHz/mT	/	/	20.2～21.8 mT	/	[40]
PM-IM OEO	GMM-PS-FBG(AC)	1.14 rad/nT@2 000 Hz	0.509 pT/Hz$^{1/2}$	/	500～10 kHz	/	/
Single-loop OEO	Prestressed and premagnetized FBG package	3 920 Hz/mT	/	/	60～81 mT	/	[41]
Dual-loop OEO	Etched FBG filled with MF	16.3 Hz/Oe	/	/	5～10 mT	/	[42]
Vernier-effect dual-loop OEO	GMM-FBG and Monel-400-FBG	8 kHz/mT	/	529 Hz/℃	50～100 mT	/	[43]
MZI-OEO	Temperature-matched MZI	1.33 MHz/mT	/	/	20～60 mT	120 kHz drift over 20 ℃	[44]
ELM-OEO	GMM-MZI	683 kHz/mT	/	5.37 MHz/℃	20～65 mT	Three times improvement in sensing accuracy	[45]
MZI-OEO	GMM-MZI (AC)	12 rad/mT	1 nT/Hz$^{1/2}$	/	1 k～14 kHz	/	/
Temperature-compensated dual-loop OEO	GMM-FBG	250 Hz/Oe	/	1.97 kHz/℃	240～760 Oe	/	[46]
Dual-loop OEO	MF immersed MI	−1.508 kHz/mT	/	/	6.69～8.35 mT	/	[47]
COEO	Magneto-optical crystal	Quadratic dependence	/	/	243～640.7 Oe	/	[48]
Single-loop OEO	GMM-FBG (AC)	327.3 rad/mT	4.65 nT/Hz$^{1/2}$	/	100～9 600 Hz	/	[49]
COEO	GMM-FBG (AC)	3.64 rad/mT	24.78 nT/Hz$^{1/2}$	/	240～10 100 Hz	/	/

工作及其性能指标。值得注意，基于OEO的磁场传感方案通常依赖闭环振荡结构，其系统稳定性和解调精度对环路参数和噪声抑制提出了较高要求。相比之下，基于MPF的磁场传感技术更多依托幅频响应或通带特性的变化进行磁场解调，在系统结构、测量维度及工程实现方面具有不同的技术特点。下面将对基于MPF的微波光子磁场传感技术进行系统综述。

1.3 基于MPF的磁场传感技术

MPF依托光学器件所具备的超宽带、低插入损耗以及优异的可调谐特性，为高性能磁场传感提供了思路[50]。基于MPF的磁场传感系统通常由光源、EOM、光纤磁场传感单元以及PD构成，如图6所示。在该类系统中，经EOM调制后的光信号在光纤磁场传感单元中与外加磁场相互作用，其光谱特性（如相位、强度或干涉条件）随外加磁场发生变化。经PD进行光电转换后，磁场信息被映射为MPF幅频响应或通带中心频率的可测漂移。结合矢量网络分析仪（Vector Network Analyzer，VNA）对MPF传输特性进行实时追踪，即可实现对磁场信息的高精度解调。

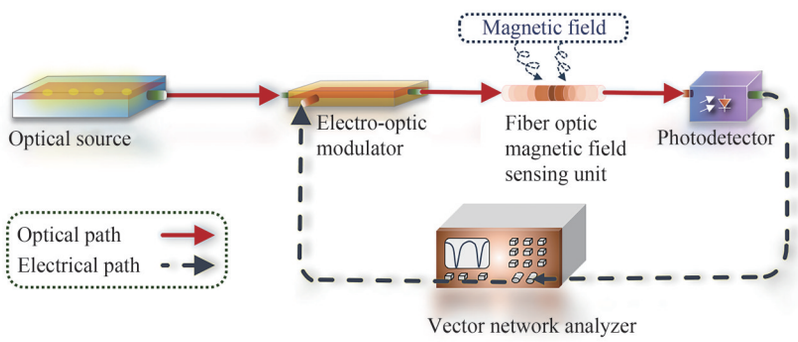

图6 基于MPF的磁场传感系统

Fig.6 Magnetic field sensing system based on MPF

MPF磁场传感的核心在于将磁场诱导的光谱偏移映射为滤波器中心频率的线性漂移。刘仟等提出了一种基于MPF的复合腔法布里-珀罗干涉仪（Fabry-Perot Interferometer，FPI）磁场传感方案。该工作采用SMF与陶瓷插芯构建复合腔FPI，并将其粘贴于GMM表面形成磁场传感单元，如图7(a)所示。实验表明，在20～70 mT磁场范围内的响应度为374.9 kHz/mT。在40～70 ℃范围内温度响应度为607.9 kHz/℃[51]。YAO Yucheng等提出基于MPF的非本征FPI传感结构，在11.424～24.276 mT范围内实现了4.61 MHz/mT的磁场响应度与54.23 μT的分辨率，验证了该类结构在小型化与高精度测量中的潜力[52]，如图7(b)所示。FENG Danqi等提出了一种串联两个光纤环（fiber ring，FR）的MPF磁场传感系统，通过在FR中嵌入线性啁啾FBG提供时间延迟，利用游标效应使微小的磁场变化被放大为显著的频率偏移[53]，如图7(c)所示。实验表明磁场响应度为127.71 kHz/Oe，放大倍数高达432。

为实现磁场与温度的同步解调，LEI Run等进一步提出并联双FR的MPF结构，通过WDM分离两路FBG反射信号，同时获得58.3 kHz/Oe的磁场响应度与1.83 kHz/℃的温度响应度[54]，如图7(d)所示。本课题组提出了一种基于保偏光纤的MPF磁场传感系统[55]，其结构由GMM及粘贴于其表面的保偏光纤构成，如图7(e)所示。外加磁场通过磁致伸缩效应调制保偏光纤的双折射特性，从而引起MPF衰落频率变化；温度变化则通过偏振复用环路中光纤的热致形变表现为滤波器下陷频率漂移。实验结果表明，在36～93.6 mT磁场范围内系统磁场响应度为5.72 MHz/mT，在32～37 ℃温度范围内温度响应度达到3.527 MHz/℃，实现了高响应度的磁场温度双参量感知。

三维矢量磁场测量可通过光载微波干涉（Optical Carrier-Based Microwave Interferometry，OCMI）技术实现。该技术利用VNA采集多抽头MPF频率响应并进行逆傅里叶变换，重构各反射点的时域干涉信号以获取三维磁场信息。本课题组提出一种基于OCMI的低反射率光纤布拉格光栅（Low Reflectivity Fiber Bragg Grating，LRFBG）阵列的磁场传感系统，将X、Y、Z三个磁场单元与双波长温度补偿单元集成为五抽头MPF[56]，如图8(a)所示。在1～10 mT范围内实现了3.2 MHz/mT的磁场响应度与7 μT的分辨率，温度响应度为0.3 MHz/℃。为了满足交变磁场的矢量测量需求，本课题组进一步提出了基于LRFBG阵列的磁

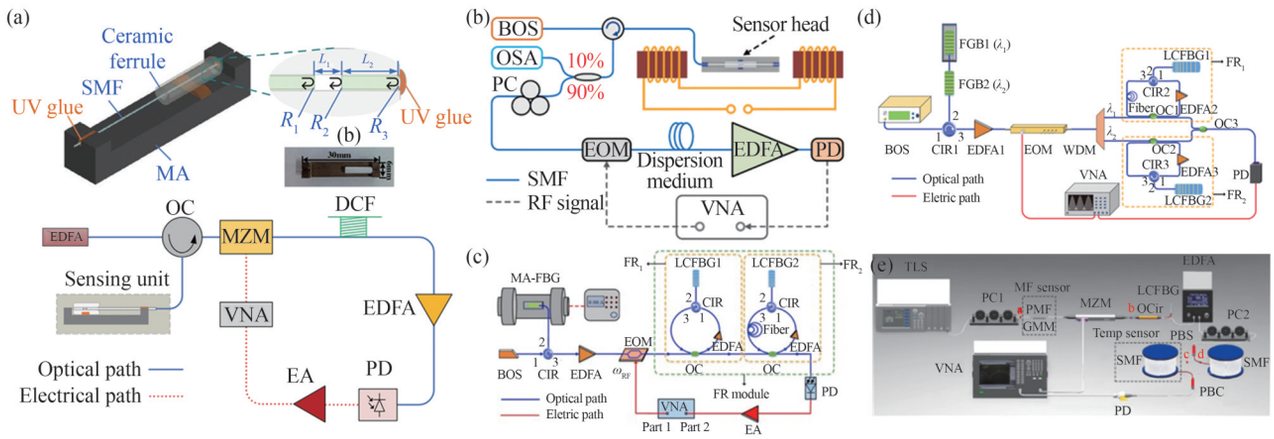

图7 基于MPF的磁场传感结构。(a)基于复合腔FPI的MPF传感结构[51];(b)基于非本征FPI的MPF结构[52];(c)级联双FR的MPF结构[53];(d)并联双FR的MPF结构[54];(e)基于保偏光纤的MPF传感系统[55]

Fig. 7 MPF-based magnetic field sensing structures. (a) MPF sensing structure based on composite cavity FPI[51]; (b) MPF structure based on extrinsic FPI[52]; (c) MPF structure with cascaded dual FR[53]; (d) MPF structure with parallel dual FR[54]; (e) MPF sensing system based on polarization-maintaining fiber[55]

场传感系统,四个间隔10 m的LRFBG反射点构成磁场传感阵列,如图8(b)所示。在0~12 mT、1~10 kHz范围内实现了195 nT/Hz$^{1/2}$的最佳磁场灵敏度,展示了其在三维矢量磁场监测中的潜力。

此外,本课题组提出了一种温度不敏感的OCMI磁场增敏传感方案[57],如图8(c)所示。该系统基于非相干多抽头MPF架构,通过级联FBG与三臂MZI引入多时延干涉路径,并在微波域重构光学干涉频谱以实现高灵敏磁场传感。磁场与温度分别对应不同的游标效应工作模式:磁场测量采用增强型游标效应,以放大微小波长偏移;温度测量则采用减小型游标效应,从而有效抑制热漂移影响。通过跟踪叠加包络下陷峰的频率漂移,可实现磁场与温度的独立解调,在0~50 mT范围内磁场响应度达6.79 MHz/mT,而在35~39.5 ℃范围内温度响应度仅为0.04 MHz/℃。稳定性测试显示最大频率漂移约为0.2 MHz,对应磁场测量精度约25.6 μT。该方案在保持高灵敏度的同时显著抑制了温度串扰,为复杂环境下的高精度磁场测量提供了有效途径。

综上所述,基于MPF的微波光子磁场传感技术充分利用了光域频率响应与微波域相干解调的优势,实现了从单点到多维的多场景磁场测量。通过结构优化、游标效应增敏及OCMI干涉重构等手段,可在保持

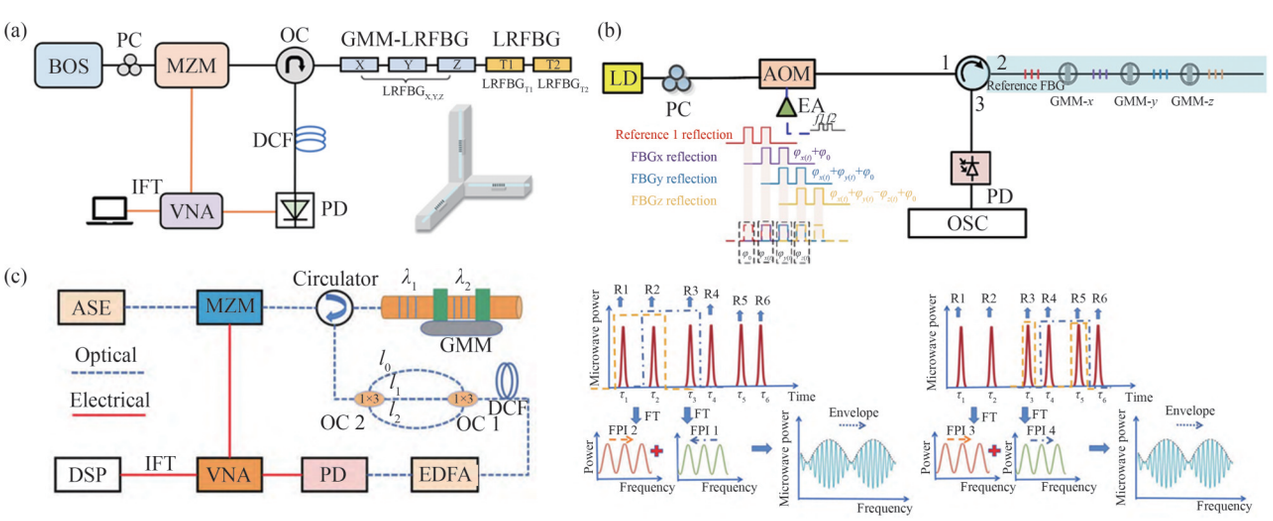

图8 矢量磁场传感系统结构与温度串扰抑制方案。(a)基于OCMI的三维磁场传感系统[56];(b)基于LRFBG的矢量交变磁场测量方案结构;(c)基于游标效应的温度不敏感磁场传感结构及磁场、温度解调过程[57]

Fig.8 Vector magnetic field sensing system architectures and temperature crosstalk suppression schemes. (a) A three-dimensional magnetic field sensing system based on OCMI[56]; (b) The structure of the vector AC magnetic field measurement scheme of LRFBG; (c) The temperature-insensitive magnetic field sensing structure based on vernier effect and the magnetic field and temperature demodulation process[57]

高响应度的同时兼顾温度稳定性与系统集成度，为未来多参量、矢量化及准分布式磁场传感的发展提供了重要技术路径。表2汇总了部分代表性工作及其性能参数。与基于OEO的磁场传感方案相比，基于MPF的磁场传感方案通常以幅频响应或通带中心频率漂移作为解调量，易于与VNA等成熟微波测量设备结合，在多参量解耦及三维磁场测量方面具有优势。相比之下，基于OEO的磁场传感方案更适用于单点磁场测量，可结合频率或相位提取算法实现高灵敏度磁场解调，适合弱磁场检测等应用场景。两类技术路线在解调机制、系统复杂度及应用侧重点方面具有良好的互补性，为不同应用需求下的微波光子磁场传感系统设计提供了多样化的实现思路。

表2　基于MPF的微波光子磁场传感技术参数对比

Table 2　Comparison of microwave photon magnetic field sensing technology parameters based on MPF

Scheme	Sensing structure	Magnetic field responsivity	Magnetic field sensitivity	Temperature responsivity	Magnetic field range	References
PM-IM MPF	EFPI	374.9 kHz/mT	/	607.9 kHz/℃	20～70 mT	[51]
EFPI-MPF	EFPI	4.61 MHz/mT	/	/	11.424～24.276 mT	[52]
Cascaded dual-FR MPF	GMM-FBG	127.71 kHz/Oe	/	1.83 kHz/℃	240～1 000 Oe	[53]
Parallel dual-FR MPF	GMM-FBG	58.3 kHz/Oe	/	1.83 kHz/℃	240～550 Oe	[54]
PMF-based MPF	GMM-PMF	5.72 MHz/mT	/	3.527 MHz/℃	36～93.6 mT	[55]
OCMI	GMM-LRFBG array	3.2 MHz/mT	/	0.3 MHz/℃	1～10 mT	[56]
OCMI	GMM-FBG array	6.79 MHz/mT	/	0.04 MHz/℃	0～50 mT	[57]
Dual optical-pulse interferometry	GMM-LRFBG array	1.2 rad/mT	195 nT/$Hz^{1/2}$	/	1 k～10 kHz	/

2　磁场解调后处理技术

微波光子磁场传感系统的最终测量精度不仅取决于光纤传感单元本身的灵敏度，其性能还会受到磁-光换能材料的非理想特性、温度交叉敏感性以及系统噪声等因素的共同限制。具体而言，磁场换能器本身存在磁滞、温度依赖、老化退化等非线性效应，光纤与磁敏元件热膨胀系数不匹配会引入温漂误差，封装结构在机械振动下会向光纤耦合低频扰动，从而在解调链路中表现为额外的系统噪声并降低信噪比。典型换能器的主要非理想因素如表3所示。为抑制上述多源误差，通常采用两类策略。其一是系统级补偿设计，例如引入温度补偿通道、双参量测量单元、差分参考路径等，以降低温漂和交叉敏感。该部分在上一节已有论述。其二是算法后处理，包括磁滞补偿和非线性修正，以利用算法在解调阶段进一步提升测量精度和鲁棒性。本节将重点围绕磁滞效应与系统噪声分别介绍其相应的后处理方法。

表3　不同磁场换能器的非线性效应

Table 3　Nonlinear effects of different magnetic field transducers

Transducer type	Non-ideal factors	Key impact on sensing performance	Practical challenges
Magnetostrictive materials	Hysteresis, temperature sensitivity, mechanical fatigue	Energy loss, nonlinear response, reduced accuracy	Limited long-term stability
Magnetic fluids	Temperature sensitivity, oxidation-induced performance degradation	Accuracy degradation, decay of magnetic properties	Limited long-term stability
Magneto-optical materials	Hysteresis, temperature dependence of Verdet constant	Accuracy degradation, increased optical loss	Limited long-term stability, stringent temperature control

磁致伸缩材料与磁光材料等磁敏换能介质往往呈现显著的磁滞特性，表现为输出与磁场输入之间存在非线性、非单值和路径依赖。磁滞不仅会引入静态测量误差，也会在动态测量中造成迟滞滞后和幅度压缩。因此，对磁滞进行补偿是实现高精度磁场测量的关键环节。目前主要有三类思路：基于解析模型的补偿、基于神经网络的学习预测以及基于迭代策略的在线校正。

基于解析模型的补偿方法是建立可逆的、参数化的迟滞模型，并将其逆模型用作前馈补偿器。典型模

型包括Preisach模型、Prandtl-Ishlinskii (PI)模型及其改进形式。早期工作中,BERENYI P等在2003年提出结合简化Preisach模型和神经网络的方法,用于在线识别磁性材料的非局部记忆型迟滞并进行补偿,实现了优于5%的建模误差,并通过实验验证了实时可行性[58]。2013年,ZONG Xiaoping等提出基于Preisach逆模型的前馈补偿策略[59],通过逆迟滞模型抑制迟滞非线性并结合自适应控制器维持闭环稳定,提升了压电驱动场景下的跟踪精度。WANG Xiangjiang等在2012年引入Krasnosel'skii-Pokrovskii算子建立迟滞模型,并将其与滑模自适应控制相结合,用于动态迟滞补偿[60],在快速变化磁场的情况下仍保持较好的跟踪性能。DONG Ruili在2014年提出将扩展输入空间的外生输入的非线性自回归移动平均模型用于描述传感器迟滞行为,并构建逆模型补偿器[61],补偿后输入-输出关系显著线性化,动态漂移也被抑制。SU Liangcai等提出基于显式迟滞模型的逆补偿方法,并将其与扰动估计触发控制框架结合,提高了非线性迟滞系统在外扰下的抗扰动能力[62]。

PI模型由于结构清晰、可逆性好、适合集成到实时控制中,被频繁用于磁致伸缩执行器、压电执行器等场景。2008年,JANOCHA H等基于改进的PI模型实现了可编程逻辑门阵列的硬件级实时迟滞补偿器,将1 kHz以内信号的非线性度从约26%降低至1.2%,证明了高速补偿的可行性[63]。随后,GU Guoying等于2012年提出实时逆PI补偿方法[64],通过直接建模逆迟滞特性并将其置于前馈通道,可将迟滞引起的误差削减约90%,可直接用于实时控制。为了应对高频动态迟滞和非对称迟滞行为,WANG Wen在2021年提出动态延迟PI模型[65],提升了对压电执行器在高频条件下不对称/动态迟滞的响应能力。实验显示,该模型在高频段的最大绝对误差较传统模型下降约80%,补偿后非线性误差可由36%降低至5.0%。2022年,AN Dong等提出的分离级环PI模型通过逻辑划分并单独建模复杂迟滞回线,可将复杂迟滞场景下的补偿精度提升约50.3%[66]。同年,ZHOU Chao提出的双算子改进PI模型针对非对称迟滞进行补偿[67],使得补偿后的均方根误差降至0.56 μm,较标准PI模型降低约93%。

此外,基于神经网络或学习型模型的补偿方案也被广泛研究。其核心思想是通过神经网络直接学习迟滞的正向和逆向映射关系,从而进行预测与前馈校正。SUN Ying等利用动态递归神经网络(Dynamic Recurrent Neural Network, DRNN)同时构建动态迟滞估计器和前馈补偿器[68],用于刻画与补偿GMM中的迟滞和速率相关特性,从而提高跟踪精度,如图9所示。CAO Shuying同年将DRNN与比例-微分控制器结合,提出在线迟滞补偿策略[69],将GMM的非线性度由约26%降至约1.2%。WANG Xiaodong等还提出利用支持向量机对迟滞和非线性误差进行两阶段补偿—补偿迟滞后再次补偿残余非线性[70],从而显著改善了长期稳定性,并优于传统基于遗传算法优化的BP方法。2014年,JI Huawei等采用BP神经网络对迟滞建模,并比较了纯反馈比例积分控制、前馈补偿和复合控制三种方案的控制性能,实验结果表明复合控制可显著削弱迟滞影响[71]。WANG Chuanli等于2021年结合GMM的双向能量转换机理,提出基于偏置电流的输出补偿方法,并利用基于甲虫触角搜索算法优化的BP网络建立迟滞模型[72],将传感器线性度由1.9%提升至1.6%,同时提高了灵敏度约1.4倍。

迭代式校正方法利用"测量-修正-再驱动"的闭环过程逐步抵消迟滞带来的误差,该类方法不依赖精确

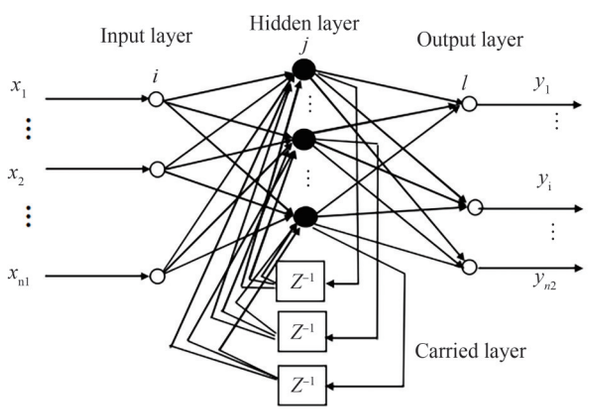

图9 DRNN结构[68]

Fig.9 Structure of the DRNN[68]

的解析模型。TSENG C等提出迭代补偿算法[73]，测得的反馈位置信号为约束，在每一迭代周期中更新驱动指令。该方法克服了直接构造逆迟滞算子在数学建模上的复杂性，且在实验中仅需少量迭代即可消除压电执行器的迟滞误差。这些补偿策略已从静态建模走向动态建模，从单一模型走向复合模型，并逐步具备在线、实时和自适应能力，从而缓解基于磁场换能器的光纤传感系统的迟滞与漂移问题。

综上所述，针对磁致伸缩与磁光换能介质固有的迟滞非线性问题，研究者已发展出以解析模型、神经网络模型及迭代校正为代表的多类磁滞补偿策略。基于解析模型的策略具有物理意义清晰、可逆性好等优势，适合嵌入实时解调与控制环路。基于神经网络模型的方案在刻画复杂、强非线性和多变量耦合迟滞行为方面表现出更强的建模能力。迭代式校正策略则在不依赖精确模型的前提下，为在线自适应补偿提供了简洁有效的实现途径。后处理技术正由“静态建模”向“动态自适应”演进，并逐步与微波光子磁场传感系统的解调链路深度融合。上述进展为抑制迟滞引入的测量偏差、提升磁场解调精度与长期稳定性提供了重要支撑，也为复杂环境下高精度磁场测量奠定了基础。

3 总结与展望

本文综述了微波光子磁场传感技术的研究进展。相较于传统光学磁场结构，基于微波光子学的光纤磁场传感系统在稳定性和测量精度方面展现出显著优势。同时，该类系统在偏振不敏感性和系统成本控制方面也具有良好的应用潜力。近年来，基于OEO与MPF的磁场传感技术不断取得进展，磁场响应度已突破GHz/mT量级。通过引入双频振荡、游标效应与OCMI等机制，实现了磁-温双参量解调与三维矢量磁场高精度测量。采用臂长匹配与热膨胀系数优化材料，可有效抑制温度串扰，基于复合腔FPI与偏振复用MPF的幅度解调方案进一步实现了磁-温分离。同时，结合模型补偿、神经网络预测及迭代优化算法的后处理系统能够显著削弱非线性迟滞和噪声对测量结果的影响，显示出在能源勘探和生物医学检测等领域的潜在应用前景。

尽管微波光子磁场传感技术已取得显著进展，但其进一步发展仍受到系统集成度、多参量解耦及灵敏度极限等因素的制约。一方面，目前大多数系统仍依赖分立光电器件，光路损耗与环境敏感性较高，影响了解调精度和长期稳定性。未来需要推进光电与微波器件的单片或混合集成，实现低损耗、低成本的片上化传感与解调结构。另一方面，虽然已有磁-温双参量及三维矢量磁场测量研究，但在复杂环境中仍面临多物理场交叉敏感问题。深度学习驱动的频域特征提取算法与多功能复合传感材料的结合，有望在信号分离与精度提升方面发挥重要作用。未来可引入光学微腔增强、光子晶体结构及量子磁传感等新机制，以突破灵敏度极限并拓展应用频段。

微波光子磁场传感技术通过光域及微波域的协同调控，为高精度、多维度磁场测量提供了全新的解决思路。该技术在电力设备监测、地质勘探和生物医学检测等场景中展现出广阔的应用潜力。随着片上集成光子器件、智能信号处理算法以及新型磁光材料的持续发展，微波光子磁场传感有望在未来实现更高灵敏度、更强环境适应性与更优系统集成度，成为面向智能化磁场测量的重要支撑技术之一。

参考文献

[1] RIPKA P, JANOSEK M. Advances in magnetic field sensors[J]. IEEE Sensors Journal, 2010, 10(6): 1108-1116.

[2] LI Zehua, SHANG Junna, WEI Liao. A robust factor graph framework for navigation on PDR/magnetic field integration[J]. Measurement, 2025, 245: 116509.

[3] MURZIN D, MAPPS D J, LEVADA K, et al. Ultrasensitive magnetic field sensors for biomedical applications[J]. Sensors, 2020, 20(6): 1569.

[4] WU Fang, VIBHUTE A, SOH G S, et al. A compact magnetic field-based obstacle detection and avoidance system for miniature spherical robots[J]. Sensors, 2017, 17(6): 1231.

[5] LENZ J, EDELSTEIN S. Magnetic sensors and their applications[J]. IEEE Sensors Journal, 2006, 6(3): 631-649.

[6] QUYNH L K, HIEN N T, BINH N H, et al. Simple planar Hall effect based sensors for low-magnetic field detection[J]. Advances in Natural Sciences: Nanoscience and Nanotechnology, 2019, 10(2): 025002.

[7] LI Jiaxian, LIU Hao, BI Tianshu. Tunnel magnetoresistance-based noncontact current sensing and measurement method[J]. IEEE Transactions on Instrumentation and Measurement, 2022, 71: 1-9.

[8] TREVIZO A S, HODGE A M. Nanomaterials by design: a review of nanoscale metallic multilayers[J]. Nanotechnology, 2020, 31(29): 292002.

[9] TUMANSKI S. Modern magnetic field sensors-a review[J]. Sensors, 2013, 13(7): 9585-9604.
[10] MOGHE R, YANG Y, LAMBERT F, et al. A scoping study of electric and magnetic field energy harvesting for wireless sensor networks in power system applications[C]. IEEE Energy Conversion Congress and Exposition. 2009: 3550-3557.
[11] BAO Bo, HUA Yu, WANG Ridong, et al. Quantum-based magnetic field sensors for biosensing[J]. Advanced Quantum Technologies, 2023, 6(5): 2200146.
[12] LIU Weidong, LI Linfeng, LI Le, et al. Velocity estimation of underwater vehicle based on abnormal magnetic field waveform[J]. IEEE Sensors Journal, 2023, 24(1): 367-376.
[13] ROSTAMI A, WAHAAB F A, SOLEIMANI H, et al. Advances in fibre Bragg grating technology for magnetic field sensing: a review[J]. Measurement, 2023, 221: 113482.
[14] YIN Shiyu, LOUSTEAU J, OLIVERO M, et al. Analysis of Faraday effect in multimode tellurite glass optical fiber for magneto-optical sensing and monitoring applications[J]. Applied Optics, 2012, 51(19): 4542-4546.
[15] MIHAILOVIC P, PETRICEVIC S. Fiber optic sensors based on the Faraday effect[J]. Sensors, 2021, 21(19): 6564.
[16] ZHENG Yangzi, DONG Xinyong, CHAN C C, et al. Optical fiber magnetic field sensor based on magnetic fluid and microfiber mode interferometer[J]. Optics Communications, 2015, 336: 5-8.
[17] SHI Fuquan, LUO Yan, CHE Jiajia, et al. Optical fiber F-P magnetic field sensor based on magnetostrictive effect of magnetic fluid[J]. Optical Fiber Technology, 2018, 43: 35-40.
[18] ZHANG N M Y, DONG Xinyong, SHUM P P, et al. Magnetic field sensor based on magnetic-fluid-coated long-period fiber grating[J]. Journal of Optics, 2015, 17(6): 065402.
[19] YANG Minghong, DAI Jixiang, ZHOU Ciming, et al. Optical fiber magnetic field sensors with TbDyFe magnetostrictive thin films as sensing materials[J]. Optics Express, 2009, 17(23): 20777-20782.
[20] HERVÁS J, RICCHIUTI A L, LI Wei, et al. Microwave photonics for optical sensors[J]. IEEE Journal of Selected Topics in Quantum Electronics, 2017, 23(2): 327-339.
[21] ZHANG Xiongxing, QIAN Jiangxiao, WANG Wei, et al. Fiber-optic vector magnetic field sensors based on magnetic fluid: progress and prospect[J]. IEEE Transactions on Instrumentation and Measurement, 2024, 73: 1-11.
[22] KUMAR C, NADEEM M D, RAGHUWANSHI S K, et al. Recent advancement in microwave photonics sensing technologies: a review[J]. IEEE Sensors Journal, 2024, 24(8): 11974-11985.
[23] YAO Jianping. Microwave photonic sensors[J]. Journal of lightwave technology, 2020, 39(12): 3626-3637.
[24] YAO X S, MALEKI L. Optoelectronic oscillator for photonic systems[J]. IEEE Journal of Quantum Electronics, 1996, 32(7): 1141-1149.
[25] ZHANG Jiawei, MENG Xuan, HAN Tao, et al. Optical magnetic field sensors based on nanodielectrics: from biomedicine to IoT-based energy internet[J]. IET Nanodielectrics, 2023, 6(3): 116-129.
[26] YiwenOU, CHEN Jiaxuan, CHEN Wenjia, et al. A quasi-distributed fiber magnetic field sensor based on frequency-shifted interferometry fiber cavity ringdown technique[J]. Optics & Laser Technology, 2022, 146: 107607.
[27] LAN Tianshu, DING Baofu, LIU Bilu. Magneto-optic effect of two-dimensional materials and related applications[J]. Nano Select, 2020, 1(3): 298-310.
[28] SODHRO A H, PIRBHULAL S, DE ALBUQUERQUE V H C. Artificial intelligence-driven mechanism for edge computing-based industrial applications[J]. IEEE Transactions on Industrial Informatics, 2019, 15(7): 4235-4243.
[29] 张学孚,陆怡良. 磁通门技术[M]. 北京: 国防工业出版社, 1995: 1-4, 34-42.
[30] 张之圣,胡明,刘志刚,王文生. InSb磁敏电阻器导电机理及可靠性[J]. 半导体学报, 1996, (2): 136-140.
[31] BLANCHARD H, DE MONTMOLLIN F, HUBIN J, et al. Highly sensitive Hall sensor in CMOS technology[J]. Sensors and Actuators A: Physical, 2000, 82(1-3): 144-148.
[32] 周文生. 磁性测量原理[M]. 北京: 电子工业出版社, 1988.
[33] WU Beilei, WANG Muguang, DONG Yue, et al. Magnetic field sensor based on a dual-frequency optoelectronic oscillator using cascaded magnetostrictive alloy-fiber Bragg grating-Fabry-Perot and fiber Bragg grating-Fabry-Perot filters[J]. Optics Express, 2018, 26: 27628-27638.
[34] HERVÁS J, RICCHIUTI A L, LI Wei, et al. Microwave photonics for optical sensors[J]. IEEE Journal of Selected Topics in Quantum Electronics, 2017, 23(2): 327-339.
[35] ZOU Xihua, LIU Xinkai, LI Wangzhe, et al. Optoelectronic oscillators (OEOs) to sensing, measurement, and detection[J]. IEEE Journal of Quantum Electronics, 2015, 52(1): 1-16.
[36] TANG Jian, HAO Tengfei, Li Wei, et al. Integrated optoelectronic oscillator[J]. Optics Express, 2018, 26(9): 12257-12265.
[37] YANG Ye, JIN Yaqing, XIANG Xiao, et al. Single-photon microwave photonics[J]. Science Bulletin, 2022, 67(7): 700-706.
[38] HAO Tengfei, LIU Yanzhong, TANG Jian, et al. Recent advances in optoelectronic oscillators[J]. Advanced Photonics, 2020, 2(4): 044001.

[39] WU Beilei, CHEN Hong, XIAO Shiying, et al. Sensitivity enhancement for magnetic field sensor using an optoelectronic oscillator based on fiber Bragg grating Fabry-Perot cavity with acrylate adhesive[J]. IEEE Sensors Journal, 2024, 24(12): 19117-19124.
[40] 刘仟,高浦峰,蔡诗怡,等. 基于非本征光纤光栅法布里-珀罗滤波器与光电振荡器的高灵敏磁场传感[J]. 光学学报, 2024, 44(13): 1306005.
[41] GAO Pufeng, CAI Shiyi, LI Donghui, et al. Optical fiber magnetic field sensing based on an optoelectronic oscillator with a prestressed and pre-magnetized enhanced-responsivity structure[J]. Applied Optics, 2025, 64(25): 7594-7601.
[42] SUN Wei, LIU Xiangyu, DENG Ming. High-precision magnetic field sensor based on fiber Bragg grating and dual-loop optoelectronic oscillator[J]. Photonic Sensors, 2022, 12(4): 220419.
[43] WU Beilei, ZHAO Xiaotong, XIAO Shiying, et al. Magnetic field measurement with improved scale factor based on a dual-loop optoelectronic oscillator with Vernier effect using a cascaded GMM-FBG and Monel-400-FBG[J]. IEEE Transactions on Instrumentation and Measurement, 2024, 73: 1-11.
[44] ZHANG Naihan, WANG Muguang, WU Beilei, et al. Temperature-insensitive magnetic field sensor based on an optoelectronic oscillator merging a Mach-Zehnder interferometer[J]. IEEE Sensors Journal, 2020, 20(13): 7053-7059.
[45] CAI Shiyi, GAO Pufeng, WU Beilei, et al. High-performance magnetic field and temperature dual-parameter sensor based on neural network assisted optoelectronic oscillator[J]. Optics Communications, 2025: 132256.
[46] FENG Danqi, GAO Ya, ZHU Tao, et al. High-precision temperature-compensated magnetic field sensor based on optoelectronic oscillator[J]. Journal of Lightwave Technology, 2021, 39(8): 2559-2564.
[47] GU Sanfeng, FENG Danqi, WANG Tianqi, et al. High-precision magnetic field sensor via optoelectronic oscillator having taper-based in-line modal interferometer[J]. Sensors and Actuators A: Physical, 2023, 362: 114647.
[48] FENG Danqi, TANG Yangxu, LEI Run, et al. A polarimetric fiber ring laser incorporating a coupled optoelectronic oscillator and its application to magnetic field sensing[J]. Photonics, 2023, 10(6): 662.
[49] GAO Pufeng, CAI Shiyi, FAN Qinggeng, et al. High sensitivity alternating magnetic field sensing system based on an optoelectronic oscillator incorporating a magnetically controlled optical source[J]. IEEE Sensors Journal, 26(2): 1907-1914.
[50] YAO Jianping. Microwave photonic systems[J]. Journal of Lightwave Technology, 2022, 40(20): 6595-6607.
[51] 刘仟. 基于微波光子的高灵敏度光纤磁场传感技术研究[D]. 北京: 北京交通大学, 2024.
[52] YAO Yucheng, ZHAO Zhiyong, LIU Jing, et al. High-resolution magnetic field sensor utilizing a Fabry-Perot cavity assembled on Terfenol-D slab[J]. Journal of Lightwave Technology, 2025, 43(5): 2456-2465.
[53] FENG Danqi, LEI Run, LIU Yuwei, et al. Vector magnetic field measurement based on fiber ring microwave photonic filter with the Vernier effect[J]. Optics & Laser Technology, 2025, 181: 111767.
[54] LEI Run, GAO Ya, FENG Danqi, et al. Magnetic field measurement with temperature compensation based on a fiber ring microwave photonic filter and Vernier effect[J]. Optics Letters, 2024, 49: 5739-5742.
[55] ZHANG Naihan, WANG Muguang, GAO Pufeng, et al. Simultaneous magnetic field and temperature measurement with high resolution based on cascaded microwave photonic filters[J]. Optics Express, 2023, 31: 33003-33014.
[56] 王颖. 基于微波光子的光纤光栅三维磁场传感技术研究[D]. 北京: 北京交通大学, 2024.
[57] CHEN Hui, CAI Shiyi, GAO Pufeng, et al. Magnetic field sensing with fiber Bragg gratings using optical carrier-based microwave interferometry and vernier effect[J]. Acta Optica Sinica, 2025, 45(11): 1106001.
陈慧,蔡诗怡,高浦峰,等. 基于光载微波干涉与游标效应的光纤布拉格光栅磁场传感[J]. 光学学报, 2025, 45(11): 1106001.
[58] BERENYI P, HORVATH G, LAMPAERT V, et al. Neural networks for nonlocal hysteresis function identification and compensation[J]. IEEE Transactions on Magnetics, 2003, 39(5): 3362-3364.
[59] ZONG Xiaoping, ZHANG Na, WANG Peiguang. Study on control strategy of nonlinear systems with hysteresis inverse model feed-forward compensation based on Preisach[J]. Advanced Materials Research, 2013, 823: 261-264.
[60] WANG Xiangjiang, TANG Jisong. Research of dynamic compensation for hysteresis nonlinear[J]. Applied Mechanics and Materials, 2012, 128-129: 985-989.
[61] DONG Ruili, TAN Yonghong. Inverse hysteresis modeling and nonlinear compensation of ionic polymer metal composite sensors[C]. 11th World Congress on Intelligent Control and Automation, Shenyang, 2014.
[62] SU Liangcai, SU Qiang, ZHAO Xinlong. Inverse-compensation-based DETC for nonlinear hysteresis system with disturbance[J]. Asian Journal of Control, 2023, 25: 301-313.
[63] JANOCHA H, PESOTSKI D, KUHNEN K. FPGA-based compensator of hysteretic actuator nonlinearities for highly dynamic applications[J]. IEEE/ASME Transactions on Mechatronics, 2008, 13(1): 112-116.
[64] GU Guoying, YANG Meiju, ZHU Limin. Real-time inverse hysteresis compensation of piezoelectric actuators with a modified Prandtl-Ishlinskii model[J]. Review of Scientific Instruments, 2012, 83(6): 065106.
[65] WANG Wen, HAN Fuming, CHEN Zhanfeng, et al. Modeling and compensation for asymmetrical and dynamic hysteresis of piezoelectric actuators using a dynamic delay Prandtl-Ishlinskii model[J]. Micromachines, 2021, 12(1): 92.

[66] AN Dong, LI Ji, YANG Yixiao, et al. Compensation method for complex hysteresis characteristics on piezoelectric actuator based on separated level-loop Prandtl-Ishlinskii model[J]. Nonlinear Dynamics, 2022, 109(3): 2479-2497.
[67] ZHOU Chao, YUAN Meng, FENG Chen, et al. A modified Prandtl-Ishlinskii hysteresis model for modeling and compensating asymmetric hysteresis of piezo-actuated flexure-based systems[J]. Sensors, 2022, 22(22): 8763.
[68] SUN Ying, WANG Bowen, HUANG Wenmei, et al. Hysteresis compensation control algorithm for the giant magnetostrictive actuators[C]. IEEE International Conference on Mechatronics and Automation, 2006.
[69] CAO Shuying, WANG Bowen, ZHENG Jiaju, et al. Hysteresis compensation for giant magnetostrictive actuators using dynamic recurrent neural network[J]. IEEE Transactions on Magnetics, 2006, 42(4): 1143-1146.
[70] WANG Xiaodong, YE Meiying. Hysteresis and nonlinearity compensation of relative humidity sensor using support vector machines[J]. Sensors and Actuators B: Chemical, 2008, 129(2): 274-284.
[71] JI Huawei, LIU Maona, HU Xiaoping. Hysteresis compensation of MSMA actuators based on neural network model[J]. Key Engineering Materials, 2014, 609-610: 1260-1265.
[72] WANG Chuanli, SHI Rui, YU Caofeng, et al. Research on hysteresis modeling and compensation method of giant magnetostrictive force sensor[J]. Journal of Sensors, 2021, 2021: 2734288.
[73] TSENG C, MAYERGOYZ I, MCAVOY P, et al. Iterative compensation for hysteresis effects in positioning and tracking problems[J]. Journal of Applied Physics, 2008, 103(7): 07D902.

Recent Progress in Microwave Photonic Magnetic Field Sensing Technology (Invited)

WANG Muguang, GAO Pufeng, CAI Shiyi, FAN Qinggen, ZHANG Naihan
(*Institute of Lightwave Technology, Key Lab of all Optical Network and Advanced Telecommunication Network, Ministry of Education, Beijing Jiaotong University, Beijing* 100044, *China*)

Abstract: Magnetic field sensing is essential in applications such as power equipment monitoring, geomagnetic exploration, biomedical diagnostics, and intelligent sensing infrastructures. Although electrical magnetic sensors, including Hall-effect, magnetoresistive, fluxgate, and superconducting quantum interference device sensors, have achieved technical maturity, their deployment in complex or distributed environments is often constrained by electromagnetic interference, bulky shielding requirements, and limited scalability. By contrast, microwave photonic approaches exploit the immunity, flexibility, and low cost of optical fibers together with the high resolution and wide bandwidth of microwave-domain processing, offering a promising route toward high-performance magnetic field sensing. This paper reviews the fundamental principles and recent progress of microwave photonic magnetic field sensing technologies, with emphasis on their demodulation mechanisms and system architectures.

Two microwave photonic sensing routes have emerged as representative approaches. The first is based on the Optoelectronic Oscillator (OEO), in which the fiber-optic magnetic field sensing unit is embedded within the OEO feedback loop. In this configuration, magnetic-field-induced optical perturbations are translated into shifts in the oscillation frequency or phase of OEO. Owing to the intrinsically high-Q and low phase noise of OEOs, even minute wavelength shifts from fiber Bragg grating Fabry-Perot cavities bonded to magnetostrictive materials can be amplified into measurable frequency shifts at the MHz to GHz level. Furthermore, Mach-Zehnder interferometer assisted OEO architectures enable alternating magnetic field sensing by converting magnetostrictive phase modulation into frequency or phase variations of the OEO oscillation signal, allowing sensitivities approaching the sub-nT/Hz$^{1/2}$ level in the kHz magnetic field band. Responsivity enhancement strategies, such as the Vernier effect in dual loop OEOs and prestressed magnetostrictive packaging, have been demonstrated to improve the scale factor by more than an order of magnitude without modifying the single loop OEO configuration.

The second route is based on Microwave Photonic Filters (MPFs). In this scheme, an optical carrier is modulated by an electro-optic modulator and subsequently passes through a magnetic field sensing unit. After photodetection, the magnetic field information is retrieved by tracking the shift of the filter passband, typically using a vector network analyzer. MPF-based magnetic field sensing systems naturally support multi-tap and reconfigurable architectures, and can be applied to both static and alternating magnetic field

measurements. Advanced implementations incorporating Fabry-Perot interferometers, polarization-maintaining fibers and cascaded fiber rings, MPF-based schemes enable enhanced responsivity, dual-parameter sensing, and quasi-distributed or vector magnetic field measurement capabilities.

To render microwave photonic magnetic field sensing systems practical for engineering applications, advanced post-processing techniques are essential to mitigate nonidealities originating from both magnetic transducers and microwave photonic components. Magnetostrictive and magnetic fluid elements inherently exhibit hysteresis and temperature-dependent behavior, while fiber packaging may introduce mechanical vibrations that manifest as excess phase noise. In addition, instabilities in lasers and photodetectors can induce power and wavelength fluctuations. Model-based hysteresis compensation approaches, including Preisach and Prandtl-Ishlinskii families and their dynamic or separated loop extensions, have been shown to substantially suppress nonlinear errors and restore near-linear relationship between magnetic field and frequency. In parallel, data-driven techniques based on recurrent or feedforward neural networks, support vector machines, and hybrid model-network frameworks enable online learning of the complex coupling among magnetic field, temperature, and packaging-induced stress. These techniques enable effective suppression of nonlinear errors and adaptive decoupling of magnetic field, temperature, and packaging-induced disturbances, thereby enhancing long-term stability and measurement fidelity.

In summary, microwave photonic magnetic field sensing technology combines the low cost and lightweight of fibers with the high accuracy of microwave-domain signal processing. At the hardware level, magnetic field demodulation can be achieved through microwave photonic architectures, including high-Q OEOs and tunable multi-tap MPFs. At the digital level, hysteresis can be effectively compensated using advanced signal processing and algorithms. Most reported systems still rely on discrete optoelectronic components. This reliance increases susceptibility to optical path loss and environmental perturbations, which in turn degrades demodulation accuracy and long-term stability. Future efforts should therefore focus on monolithic or hybrid photonic microwave integration to realize low loss, low cost, and compact on-chip sensing and demodulation architectures. Through coordinated control of the optical and microwave domains, this technology offers a versatile route toward high sensitivity magnetic field measurement. With continued advances in integrated microwave photonic platforms, intelligent signal processing algorithms, and novel magnetic transduction materials, microwave photonic magnetic field sensing is expected to evolve toward higher sensitivity and stronger environmental adaptability. These developments will also promote improved system integration and support future applications in power equipment monitoring, geomagnetic exploration, and biomedical magnetic detection.

Key words: Fiber optics sensors; Magneto-optic systems; Oscillators; Spectroscopy, Microwave

OCIS Codes: 060.2370; 230.3810; 230.4910; 300.6370

CSTR: 32255.14.gzxb20265503.0355105

Foundation item: National Natural Science Foundation of China (62371035, U2006217)